Second-generation quantum-well sensors for room-temperature scanning Hall probe microscopy

A. Pross, A. I. Crisan, and S. J. Bending[a)]
Department of Physics, University of Bath, Bath BA2 7AY, United Kingdom

V. Mosser
Itron France, UTG, 50 Avenue Jean Jaurès, F-92542 Montrouge, France

M. Konczykowski
Laboratoire des Solides Irradiés, Ecole Polytechnique, 91128 Palaiseau, France

(Received 4 October 2004; accepted 15 February 2005; published online 20 April 2005)

Scanning Hall probe microscopy is a noninvasive magnetic imaging technique with potential for having a major impact in the data storage industry if high-resolution Hall effect sensors can be developed with sufficiently low-noise figures at room temperature. To meet this requirement, we have developed a series of second-generation quantum-well Hall probes whereby the careful design of an AlGaAs/InGaAs/GaAs pseudomorphic heterostructure, chip layout, metal interconnects, and passivation layers has allowed a dramatic reduction of low-frequency noise sources. In addition, the Johnson noise-limited minimum detectable fields of these sensors are more than an order of magnitude lower than those used in early microscopes. The key figures-of-merit of the sensors are presented and their performance illustrated in an imaging study of a yttrium–iron–garnet thin film at room temperature. © *2005 American Institute of Physics*. [DOI: 10.1063/1.1887828]

The rapidly increasing density of magnetic data storage media has lead to a growing demand for high-resolution magnetic imaging tools which can be used to characterize them. The instrument of choice in the data storage industry is currently the magnetic force microscope (MFM),[1] which uses the interaction force between a sharp ferromagnetic tip on a micromachined cantilever, and the stray fields of a magnetic sample, to build two-dimensional magnetic images. While the MFM is capable of high spatial resolution, it suffers from a number of potential problems. The magnetic tip is invasive and can easily perturb the domain structure of the sample being imaged. In addition, the micromagnetic state of the tip is rarely known with any confidence, and extracting quantitative information from MFM images poses major challenges. Several other scanning probe techniques have been developed in recent years to address some of these issues including scanning superconducting quantum interference device (SQUID) microscopy,[2] scanning magnetoresistive sensors,[3] and scanning Hall probe microscopy[4–9] (SHPM).[4–9] Of these, SHPM seems to have the greatest promise since the low self-fields of the Hall probe render it virtually noninvasive, and the Hall voltage generates a direct quantitative map of the out-of-plane component of magnetic induction. The spatial resolution of SHPM also now rivals MFM, and functional 50 nm semimetal Bi Hall probes patterned with a focused ion beam in a 60 nm thick polycrystalline film were recently demonstrated.[10] With the exception of this example, all other advanced SHPMs use epitaxial III-V semiconductor Hall sensors since these generally exhibit the highest carrier mobilities and lowest resistivities. The minimum detectable fields of such systems are fundamentally limited by the Johnson noise arising in the active sensor element and Hall probe voltage leads, $V_J = \sqrt{4kTR_VT\Delta f}$, where R_V is the output resistance and Δf is the measurement bandwidth. Since the III-V materials used have extremely high carrier mobilities (low sheet resistances) at low temperatures, the signal:noise ratio is generally very high, and a wide measurement bandwidth can be used under these conditions. In contrast, the room-temperature mobilities are relatively low, resistances are high and signal:noise ratios are often rather poor. As a consequence, only very narrow measurement bandwidths are possible at 300 K, a factor which has limited the attractiveness of SHPM for room-temperature imaging applications. To overcome this obstacle, many recent developments have focused on narrow gap III-V semiconductors whose small electron effective masses can lead to exceptionally high room-temperature mobilities.[7–9] For example, a 1.5 μm Hall sensor patterned in a 1 μm thick high-quality InSb epilayer has recently been demonstrated[8] with a minimum detectable field of $\sim 6\ \mathrm{mG/Hz^{0.5}}$ at 700 Hz and 300 K. While the figures of merit of these thin films are impressive, many research efforts continue to focus on sensors containing a near-surface two-dimensional carrier system, since this allows one, in principle, to achieve the highest spatial resolution. In this article, we demonstrate that the careful design of III-V epitaxial materials, as well as device layout and processing, can lead to quantum-well sensors with Johnson noise-limited minimum detectable fields more than an order of magnitude lower than in early instruments. This generation of sensors could greatly enhance the value of SHPM for room-temperature imaging applications, and lead to a rapid growth in its implementation in the data storage industry.

Our Hall sensors are patterned in a δ-doped AlGaAs/InGaAs/GaAs pseudomorphic heterostructure

[a)]Electronic mail: pyssb@bath.ac.uk

Structure	Thickness (nm)	Al or In content
GaAs undoped	10	0
AlGaAs undoped	50	graded to 0.32
Si δ-doped layer	δ-doping	$N_d = 2.5 \times 10^{12}$ cm^{-2}
AlGaAs undoped	4.5	0.32
InGaAs undoped	13	0.15
GaAs undoped buffer	1000	0
GaAs s.i. substrate	0.5mm	0

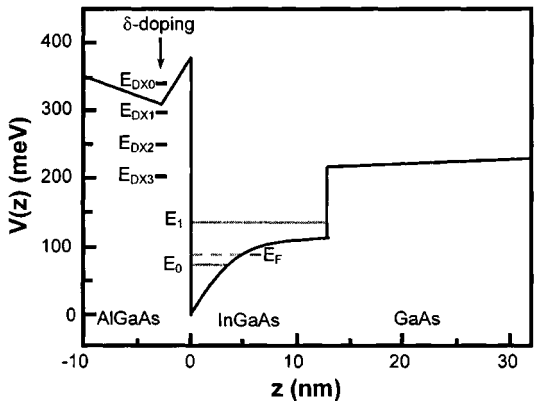

FIG. 1. (Top) MBE growth sequence of the epilayers used to fabricate the probes. (Bottom) Sketch of the band structure of the heterostructure in the vicinity of the InGaAs quantum well. Labels indicate the energies of the Fermi energy (E_F) and the zeroth (E_0) and first (E_1) subband edges in the quantum well. (E_{DXn}) indicate the energy levels of *DX* centers with *n* Al atoms among the three group-III next-nearest-neighbor atoms of the broken bond, when a Si dopant in AlGaAs is in the relaxed negatively charged *DX* state.

which was grown by Picogiga International using molecular-beam epitaxy (MBE) on a semi-insulating GaAs wafer.[11] The epilayer sequence (see table in Fig. 1) incorporates a 1 μm thick GaAs buffer, followed by a 13 nm thick $In_{0.15}Ga_{0.85}As$ quantum well, an $Al_xGa_{1-x}As$ barrier layer with graded aluminum concentration, and a 10 nm GaAs capping layer. A two-dimensional electron gas is induced by the inclusion of a Si δ-doping layer in the graded $Al_xGa_{1-x}As$ barrier, within reach of the $In_{0.15}Ga_{0.85}As$ well. The profile of this barrier is carefully tailored so that all the *DX* levels introduced by the δ-doping lie well above the Fermi level in the nearby two-dimensional electron gas in the InGaAs well. This both eliminates low-frequency noise due to carrier generation-recombination associated with *DX* centers[12] and ensures that all Si donors are fully ionized.[13] The use of δ-doping minimizes scattering by remote ionized donors (and maximizes the carrier mobility in the $In_{0.15}Ga_{0.85}As$ well) subject to the restriction that large spacer layers cannot be used if trapping at *DX* states is to be avoided. All layers, apart from the quantum well, are fully depleted of electrons and holes. The concentration of the δ-doping layer ($\sim 1\times 10^{12}$cm^{-2}) was adjusted in order to yield the required two-dimensional electron density $n_S = 8.9 \pm 0.2 \times 10^{11}$cm^{-2} in the quantum well corresponding to a sensitivity of 700 ± 20 V/AT with a very small thermal drift of less than $\pm 1\%$ in the temperature range from -40 °C to $+100$ °C. Hall sensors of various dimensions have been patterned in a van der Pauw geometry using optical lithography. Parasitic resistances and inductive pickup

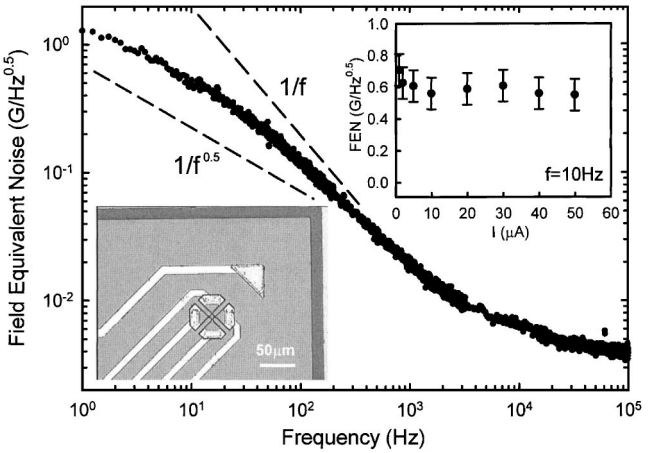

FIG. 2. Spectrum of the FEN of a typical Hall sensor at 300 K. Top inset shows the current dependence of the FEN at 10 Hz. Bottom inset shows an optical micrograph of the active corner of the Hall sensor.

have been minimized by the careful design of the Ti/Pt/Au stripline interconnects which link 100 μm bond pads at the edge of the chip to the AuGeNi Ohmic contacts, only 15 μm away from the active Hall sensor (see bottom inset of Fig. 2). Since the resistance introduced by the contact metalization is very much smaller than that of the semiconductor wires, this minimizes the series resistance of the Hall voltage leads and hence the Johnson noise floor. Finally, the surface of the Hall structure is stabilized by coating it with a plasma enhanced chemical vapor deposited SiO_2 passivation layer. Constant Fermi-level transient spectroscopy[14] has revealed that $GaAs/SiO_2$ interface states exhibit a U-shaped density of states with a minimum of $\sim 3\times 10^{12}$ cm^{-2}/eV. At a sufficiently high temperature, the interface states are in thermal equilibrium with the electrons in the quantum well resulting in Fermi-level pinning around midgap and yielding highly reproducible sensitivity and temperature coefficients. The Hall probe described here has nominal dimensions of 4 μm $\times$ 4 μm, but lateral etching during the definition of the Hall cross of $\sim 1-2$ μm at each edge reduces the effective size to less than 2 μm $\times$ 2 μm. A triangular Ti/Pt/Au scanning tunneling microscope (STM) tip has also been integrated onto the chip (top right of lower inset to Fig. 2) about 100 μm from the Hall sensor and the entire device was diced from a larger piece of wafer with a wire saw. The electron mobility of the two-dimensional electrons at 300 K is ~ 7000 cm^2/V s, typical resistances between pairs of current or voltage leads are ~ 10 kOhm and the offset voltage of the patterned device corresponds to a field of less than 10 G.

Figure 2 illustrates the measured field-equivalent noise (FEN $= V_n/(R_H I)$, where R_H is the Hall coefficient and I is the probe current) measured on a typical sensor in the range $10^0 - 10^5$Hz at a dc drive current of 40 μA. The Hall voltage has been amplified with an NF L175A preamplifier, whose output was then delivered to a commercial spectrum analyzer. The top inset to the figure illustrates that the FEN of the entire measurement system at 10 Hz is independent of drive current up to the maximum safe current of 50 μA. The observed low-frequency noise was shown in earlier studies[15] to be exactly what one expects for trapping/detrapping

within the continuum of $GaAs/SiO_2$ interface states. Low-frequency noise is related to the associated thermally activated carrier capture and emission processes, and the continuum of time constants of interface levels located within a few kT of E_F yields a smeared-Lorentzian behavior for the spectral density. From a practical point of view, this produces a $1/f^{0.5}$ dependence around 1 Hz. Above a corner frequency of about 10 kHz, the low-frequency noise falls below the Johnson noise limit which, for a typical drive current of 40 μA, is $\sim 4\ \mathrm{mG/Hz^{0.5}}$. This is comparable with the same figure of merit for the much thicker InSb thin film sensor of Ref. 8 (which exhibits somewhat lower noise levels at lower frequencies). More importantly, the location of the InGaAs quantum well about 80 nm below the surface of our structures ultimately allows a comparable spatial resolution to be achieved in nanoscale sensors. To obtain similar resolution in epitaxial InSb will require the use of much thinner films with lower carrier mobilities,[16] and it is not clear *a priori* how the noise figures would scale with device dimensions. Surprisingly, a 500 nm nanomagnetometer patterned with an Ar focused ion beam in a 320 nm thick InSb eiplayer was recently reported[17] to have approximately the same minimum detectable field as the much larger sensor of Ref. 8, suggesting that the scaling properties may be better than one might expect.

The InGaAs Hall sensor was mounted and wire bonded onto the package of a commercial scanning Hall probe microscope (NanoMagnetics Instruments Ltd). The completed package was then screwed onto the end of a piezoelectric scanner tube which was equipped with a spring pin assembly for contacting the four Hall sensor leads and the STM tip. A yttrium–iron–garnet (YIG) film with out-of-plane magnetic anisotropy was mounted on the sample puck of the inertial stick/slip approach mechanism, which hangs beneath the Hall sensor. The sample puck has three adjustable springs which allow one to set a tilt angle of $\sim 0.5°$ between the Hall probe and sample surfaces such that the tunneling tip is at the closest point. The entire microscope head was placed in a vibration-isolated cryostat equipped with a pair of Helmholtz coils capable of providing out-of-plane fields up to ±100 Oe. The sample was approached towards the Hall sensor until a tunnel current was established within a feedback loop. The sensor was then retracted a few hundred nanometers out of tunnel contact, allowing rapid Hall probe scans of the local induction to be made. Figure 3 shows a family of typical 300 K SHPM images (all sizes $\sim 52\ \mu\mathrm{m} \times 52\ \mu\mathrm{m}$) of stripe domains in the YIG sample at various applied fields in the range −20 Oe–20 Oe. A dc Hall probe current of 40 μA has been employed, the measurement bandwidth for the Hall voltage was set to 0.1 kHz and each image was scanned at the fastest speed allowed by our instrument ($\sim$150 s/image). Although the single scan images are perfectly acceptable, ten successive scans have been averaged to generate the publication quality images shown in Fig. 3. In a separate experiment, the Hall sensor was parked near the center of the scan area while the applied field was swept around a hysteresis cycle in 60 s to generate a "local" magnetization loop ($M_{\mathrm{loc}} = B_{\mathrm{loc}} - H$). A typical *M-H* loop is reproduced at the center of Fig. 3, where a measurement bandwidth of ~ 5 Hz was employed to reduce the noise level. The

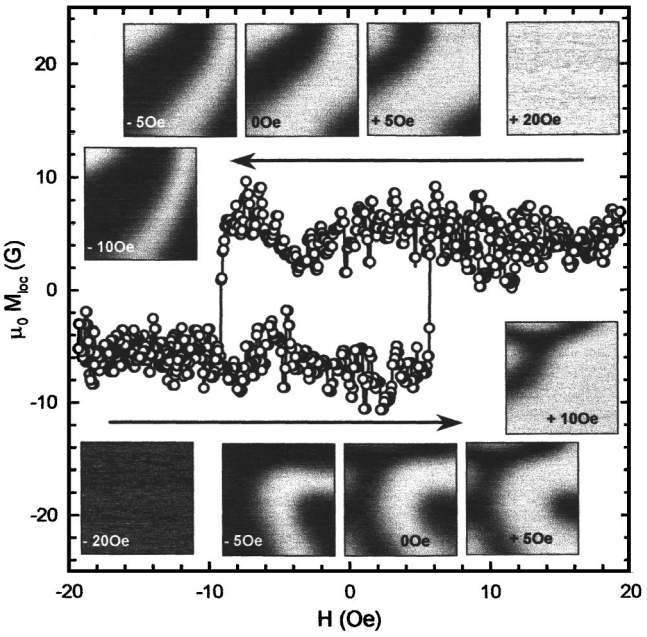

FIG. 3. Local magnetization curve ($M_{\mathrm{loc}} = B_{\mathrm{loc}} - H$) captured at 300 K with our scanning Hall sensor positioned just above a YIG film. Insets show scanning Hall probe images (all $\sim 52\ \mu\mathrm{m} \times 52\ \mu\mathrm{m}$) of the same region of the film captured around a single cycle at the indicated magnetic fields. In images where both magnetic domains are present, the grayscale spans $\sim$30 G, whereas it spans $\sim$9 G when only a single domain occurs.

inset images have been captured at different positions around the cycle and illustrate how magnetization reversal takes place by both domain growth and domain-wall motion. This gives rise to the weak mesoscopic structures seen in the local magnetization data since it depends on the domain structure both underneath as well as nearby the sensor.

In conclusion, we have demonstrated a second-generation semiconductor quantum-well Hall sensor which can operate at room temperature with a Johnson noise-limited minimum detectable field which is more than an order of magnitude smaller than early scanning sensors, and could potentially be reduced in size to form a nanoscale sensor with $\sim$80 nm spatial resolution. This is achieved by careful design of an AlGaAs/InGaAs/GaAs pseudomorphic heterostructure and chip layout to reduce low frequency noise sources as well as passivation layers to stabilize GaAs surface states. Work is underway to reduce the active sensor size to submicron dimensions when the technique of growth on a patterned substrate introduced in Ref. 6 may be invaluable for minimizing sample/sensor separation. Once development is complete, these probes should become highly attractive for a range of imaging applications in ferromagnetic materials at room temperature.

The authors are grateful to Dr. A. N. Grigorenko of the University of Manchester who provided the YIG sample for imaging. They also acknowledge the financial support of EPSRC in the UK (Grant No. GR/R18413).

[1] Y. Martin and H. K. Wickramasinghe, Appl. Phys. Lett. **50**, 1455 (1987).
[2] J. R. Kirtley, M. B. Ketchen, K. G. Stawiasz, J. Z. Sun, W. J. Gallagher, S. H. Blanton, and S. J. Wind, Appl. Phys. Lett. **66**, 1138 (1995).
[3] R. O'Barr, M. Lederman, and S. Schultz, J. Appl. Phys. **79**, 6067 (1996).
[4] A. M. Chang, H. D. Hallen, L. Harriot, H. F. Hess, H. L. Loa, J. Kao, R.

E. Miller, and T. Y. Chang, Appl. Phys. Lett. **69**, 1324 (1996).
[5]A. Oral, S. J. Bending, and M. Henini, Appl. Phys. Lett. **69**, 1324 (1996).
[6]T. Schweinbock, D. Weiss, M. Lipinski, and K. Eberl, J. Appl. Phys. **87**, 6496 (2000).
[7]J. K. Gregory, S. J. Bending, and A. Sandhu, Rev. Sci. Instrum. **73**, 3515 (2002).
[8]A. Oral, M. Kaval, M. Dede, H. Masuda, A. Okamoto, I. Shibasaki, and A. Sandhu, IEEE Trans. Magn. **38**, 2436 (2002).
[9]A. Sandhu, A. Okamato, I. Shibasaki, and A. Oral, Microelectron. Eng. **73**, 524 (2004).
[10]A. Sandhu, K. Kurosawa, M. Dede and A. Oral, Jpn. J. Appl. Phys., Part 1 **43**, 777 (2004).
[11]V. Mosser, F. Kobbi, S. Contreras, J. M. Mercy, O. Callen, J. L. Robert, S. Aboulhouda, J. Chevrier, and D. Adam, Proceedings of the Ninth International Conference on Solid State Sensors and Actuators, Transducers '97, Chicago, Ill., 16–19 June 1997.
[12]D. D. Carey, S. T. Stoddart, S. J. Bending, J. J. Harris, and C. T. Foxon, Phys. Rev. B **54**, 2813 (1996).
[13]V. Mosser, S. Contreras, S. Aboulhouda, P. Lorenzini, F. Kobbi, J. L. Robert, and K. Zekentes, Sens. Actuators, A **43**, 135 (1994).
[14]O. Callen and V. Mosser, Mater. Sci. Eng., B **80**, 142 (2001).
[15]V. Mosser, G. Jung, J. Przybytek, M. Ocio, and Y. Haddab, Proc. SPIE **5115**, 183 (2003).
[16]A. Okamoto and I. Shibasaki, J. Cryst. Growth **251**, 560 (2003).
[17]A. Sandhu, A. Sanbonsugi, I. Shibasaki, M. Abe, and H. Handa, Jpn. J. Appl. Phys., Part 2 **43**, L868 (2004).